

A supersonic beam of cold lithium hydride molecules

S. K. Tokunaga, J. O. Stack, J. J. Hudson, B. E. Sauer, E. A. Hinds, and M. R. Tarbutt*
Centre for Cold Matter, Blackett Laboratory, Imperial College London, SW7 2BW, United Kingdom
 (Dated: March 31, 2022)

We have developed a source of cold LiH molecules for Stark deceleration and trapping experiments. Lithium metal is ablated from a solid target into a supersonically expanding carrier gas. The translational, rotational and vibrational temperatures are 0.9 ± 0.1 K, 5.9 ± 0.5 K and 468 ± 17 K respectively. Although they have not reached thermal equilibrium with the carrier gas, we estimate that 90% of the LiH molecules are in the ground state, $X^1\Sigma^+(v=0, J=0)$. With a single 7 ns ablation pulse, the number of molecules in the ground state is $4.5 \pm 1.8 \times 10^7$ molecules per steradian. A second, delayed, ablation pulse produces another LiH beam in a different part of the same gas pulse, thereby almost doubling the signal. A long pulse, lasting $150 \mu\text{s}$, can make the beam up to 15 times more intense.

PACS numbers: 39.10.+j

I. INTRODUCTION

Techniques are currently being developed to form cold and ultracold molecules for applications across many fields of research [1, 2]. The applications include tests of fundamental symmetries and time variation of fundamental constants, quantum information processing, quantum chemistry and the physics of dipolar quantum degenerate gases. Cold molecules have more to offer than cold atoms, because of their vibrational and rotational structure. Polar molecules are of particular interest, their interaction with electric fields being typically 2-4 orders of magnitude larger than that of atoms. This interaction is the basis of an important technique for producing cold molecules, known as Stark deceleration [3]. Molecules seeded in a gas pulse are cooled by supersonic expansion to temperatures of order 1 K, but have a centre-of-mass velocity of several hundred m/s. This is reduced in the Stark decelerator by a time-varying inhomogeneous electric field. Once brought to rest, the molecules can be loaded into a trap [4] or a storage ring [5]. To date, the deceleration technique has been applied to isotopic species of CO [3], NH₃ [4], OH [6, 7], NH [8], H₂CO [9] and, in our laboratory, YbF [10]. The ratio, R , of Stark shift to mass serves as a figure of merit for Stark deceleration. At 200 kV/cm, $R = 0.189 \text{ cm}^{-1}/\text{amu}$ for OH and $0.114 \text{ cm}^{-1}/\text{amu}$ for ND₃, the only two species to have been brought to rest and trapped so far. It is a major challenge to form beams of cold molecules that have suitably large values of R at practical electric field strengths. The easiest molecules to produce at low temperature using a supersonic expansion technique are those that have substantial vapour pressure at room temperature. However, many of these are unsuitable for deceleration because R is too low. Conversely, those species that are most amenable to deceleration may be difficult to produce in the first instance. The lithium hydride molecule

falls into this second class. It is an excellent candidate for Stark deceleration, having $R = 0.388 \text{ cm}^{-1}/\text{amu}$ at 200 kV/cm. However, despite the large volume of literature on LiH, there are no reports of low temperature beams.

The spectroscopy of lithium hydride has been very extensively studied, both theoretically and experimentally, over many decades. LiH is sufficiently simple that highly accurate *ab initio* calculations of its energy level structure and physical properties are possible. For this reason, and because of its low mass, it is an excellent system for studying the breakdown of the Born-Oppenheimer approximation [11, 12]. LiH is also of considerable astrophysical interest, particularly for its role in the evolution of the early universe [13, 14]. In 1993, Stwalley and Zemke published a comprehensive review of experimental and theoretical work on the three lowest electronic states of LiH: $X^1\Sigma^+$, $A^1\Sigma^+$ and $B^1\Pi$ [15]. More recent studies include extensive sub-Doppler laser spectroscopy of the A-X system [16], high precision studies of the ground-state by emission spectroscopy in the far and mid-infrared [12, 17], and the first observation and characterization of the $C^1\Sigma^+$ state [18, 19]. All the experimental studies of gas-phase LiH have used hot sources. The molecules were either studied directly inside a heated cell, or an effusive beam was formed, usually by passing hydrogen gas through a vapour of lithium produced inside a heated crucible. A supersonic expansion source of LiH was also developed, but the rotational temperature of the molecules produced was approximately 600 K, far higher than anticipated [20]. The formation of the molecule in the gas-phase is difficult because, although the overall reaction $\text{Li} + (1/2)\text{H}_2 \rightarrow \text{LiH}$ is exothermic by 0.21 eV, the single-step reaction $\text{Li} + \text{H}_2 \rightarrow \text{LiH} + \text{H}$ is endothermic by 2.05 eV when the reactants are in their ground states [21]. One is thus faced with the challenge of producing the molecules at low temperatures while simultaneously overcoming the 24000 K barrier to the reaction. In this paper, we report the successful production of sub-Kelvin LiH beams.

*Electronic address: m.tarbutt@imperial.ac.uk

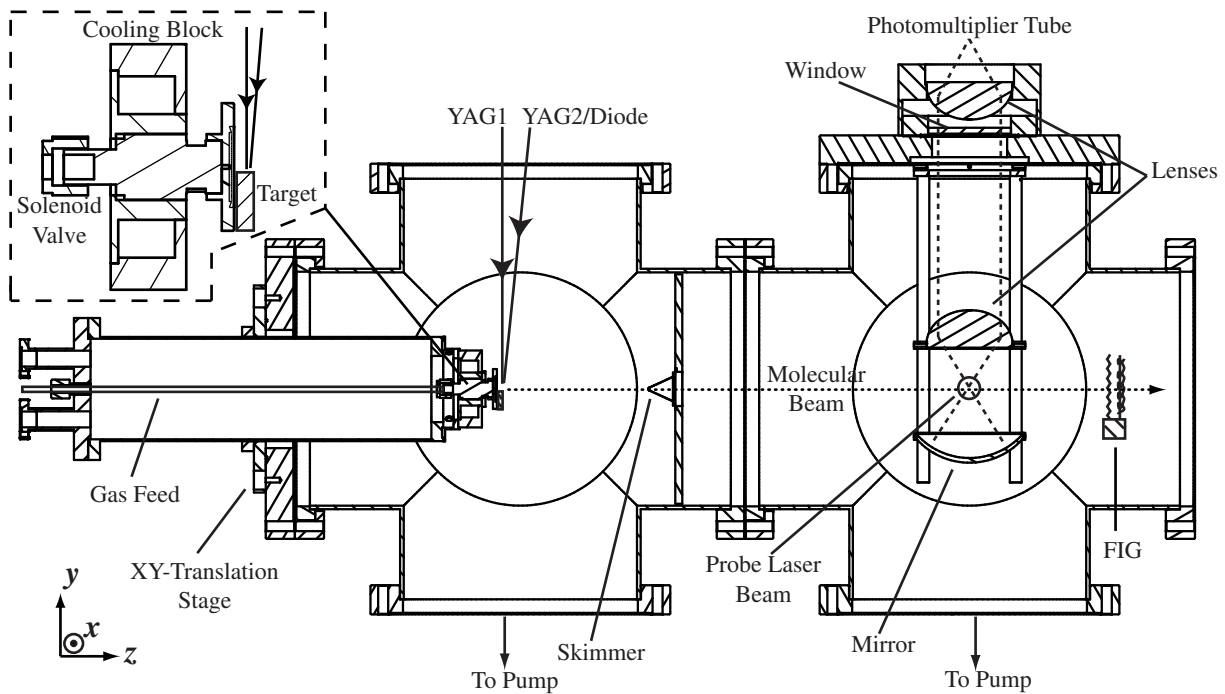


FIG. 1: Layout of the experiment and magnification of the source region (inset). YAG1 is the primary Nd:YAG laser used for laser ablation of the target. YAG2/Diode indicates the beam-path of either (i) a second Nd:YAG laser used for dual-pulse ablation experiments or (ii) a diode laser resonant with the $\text{Li } 2s - 2p$ transition. The probe laser beam propagates into the page, along x .

II. EXPERIMENT SETUP

The experimental setup is shown in Fig. 1. The vacuum system consists of two DN200CF 6-way crosses, evacuated by two 10001/s turbomolecular pumps and separated by a skimmer with a 2 mm diameter opening. A solenoid valve with a 1 mm diameter nozzle (General Valve, Series 99) is inserted into the source chamber and holds the carrier gas at a pressure in the range 2-6 bar. A voltage pulse of typical amplitude 250 V and typical duration $300 \mu\text{s}$ is applied to the valve, and a pulse of gas is emitted with an approximately Gaussian profile whose length is $\sim 100 \mu\text{s}$ [22]. When operated at 10 Hz repetition rate, as in all our experiments, the time-averaged pressures in source and detection chambers are 10^{-4} mbar and 3×10^{-7} mbar respectively. The temperature of the solenoid valve can be controlled with 1 K precision in the range 100-293 K, by regulating a flow of nitrogen gas through a cooling block that surrounds the valve. This assembly is mounted on the end of a tube, allowing the insertion depth of the valve and hence the distance from valve to skimmer to be varied. For the experiments reported below, we fixed this distance at 110 mm. The transverse position of the entire valve assembly can be adjusted under vacuum.

The LiH molecules are produced by laser ablation of a solid Li target mounted directly onto the face of the valve, and displaced from the nozzle by approximately 1 mm along $-y$ (see Fig.1). The target is ablated using

light from a pulsed Nd:YAG laser (YAG1) providing up to 450 mJ of energy at 1064 nm or 110 mJ at 355 nm in a 7 ns pulse (Q-switched mode) or a train of $1 \mu\text{s}$ pulses lasting for approximately $150 \mu\text{s}$ (long-pulse mode). To investigate dual-pulse laser-ablation, light from a second 10 ns, 1064 nm Nd:YAG laser (YAG2), is introduced at a small angle to the first. The delays between valve, YAG1 and YAG2 triggers are computer-controlled with 50 ns resolution.

The pulsed molecular beam passes through the skimmer into the detection chamber. Here it encounters the LiH detector 271 mm downstream of the skimmer. A fast ionization gauge (FIG) situated 59 mm further downstream measures the temporal profile of the gas pulse with a resolution of $5 \mu\text{s}$.

In the LiH detector, the molecules are detected by time-resolved laser-induced fluorescence in the ultra-violet (uv). The laser system consists of a single-mode cw Ti:Sapphire laser (Coherent MBR110) pumped by an 8W Nd:YVO₄ laser (Coherent Verdi V8) and frequency-doubled inside a build-up cavity (Coherent MBD200). The laser frequency is measured to an accuracy of 600 MHz using a wavemeter (HighFinesse WS-6). The probe laser beam propagating along x and linearly polarized along z , excites LiH on single rotational components of the $A^1\Sigma^+(v') - X^1\Sigma^+(v'' = 0)$ transitions. The choice of A-state vibrational quantum number, v' , is based on the efficiency for driving the transition with the laser power available. With increasing v' (in the range

$v' = 0-8$), the required laser power decreases due to the improving Franck-Condon overlaps, but the power available from the laser system also decreases as the transition frequency moves deeper into the ultra-violet. In our experiments, we have used $v' = 2, 3, 4$ at wavelengths of 376.8, 372.0 and 367.2 nm respectively. The upper state radiative lifetime is ≈ 30 ns, and non-radiative decay processes are negligible [23]. The spectrum of the resulting fluorescence will contain discrete lines with significant intensity ranging from the excitation wavelength in the uv out to 1100 nm. Light-collecting optics, consisting of a spherical mirror (90 mm diameter, 30 mm focal length) and two condenser lenses (73 mm diameter, 55 mm focal length), form a 1:1 image of this fluorescence at the 8 mm \times 24 mm photocathode of a photomultiplier tube (PMT, Hamamatsu R928P) operated in photon-counting mode and aligned with the long axis parallel to x . Scattered laser light is suppressed using a glass filter (Schott GG400) placed in front of the photocathode. On the $v' = 3$ transition, this filter transmits $< 10^{-5}$ of the photons at the laser frequency, while transmitting 73% of all the fluorescence. The photon rate at the PMT is measured as a function of the time since firing YAG1, with up to 1 μ s resolution. The resulting time-of-flight (TOF) profile provides a measurement of the molecules' speed and translational temperature, and the relative intensity of rotational lines in the spectrum measures the rotational temperature.

In addition to the probe laser system described above, we also use a 10 mW, 670 nm diode laser (Hitachi HL6714G) tuned to the D1 or D2 resonance lines of atomic lithium. This laser has two uses. In the detection region, it serves as a probe laser for lithium, allowing us to measure the Li flux in the beam. When directed onto the target, it allows us to investigate the formation of LiH by the reaction of excited-state Li with H_2 .

III. RESULTS

A. Single-pulse ablation

We begin by discussing the particular case of single-pulse 1064 nm laser ablation of a Li target into a carrier gas of Ar(98%)/ H_2 (2%) at 3 bar stagnation pressure and 293 K stagnation temperature. The ablation laser is Q-switched, providing a 7 ns pulse. Figure 2 shows the typical signal observed on the fast-ionization gauge under these conditions. To produce this data, we modulated between YAG1-off (solid line) and YAG1-on (dashed line). The data shows that the ablation process results in a local 'hole' in the gas pulse. The depth and width of this hole increases with increasing YAG1 power, and the position of the hole relative to the centre of the gas pulse is fixed by the time delay between valve and YAG1 triggers. For the data shown, this time delay was chosen to be 485 μ s in order to place the hole near the centre of the gas pulse. It is known that, following ablation, the plume forms and

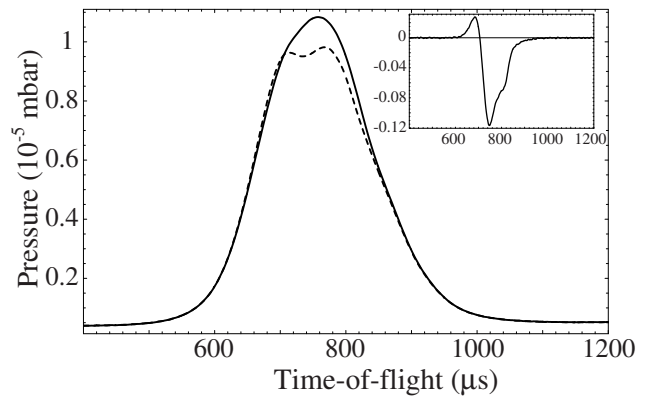


FIG. 2: Gas pulse measured on the fast-ionization gauge with Nd:YAG turned off (solid line) and on (dashed line). The inset shows the difference between the two profiles.

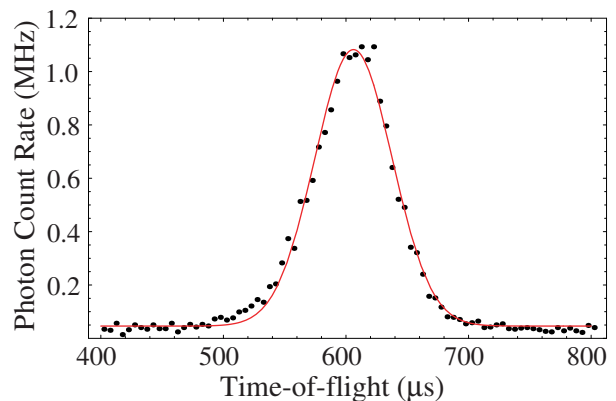


FIG. 3: LiH time-of-flight profile and gaussian fit.

propagates to the gas jet on a sub-microsecond timescale [24]. We therefore take the trigger for YAG1 as marking the moment when the hole is formed. This is the origin of time in Fig. 2. The arrival time of the gas pulse at the FIG determines its central speed as 582 m/s. As in other experiments using this type of valve, this speed is a little higher than the expected terminal speed for an ideal supersonic expansion of the gas, which is 557 m/s. The inset in Fig. 2 is the difference between the signal with the ablation laser on and off. It shows a small increase in the gas density at short times, followed by a much larger decrease at longer times. Collisions between the hot, energetic ablation plume and the gas pulse result in a loss of atoms from the carrier gas pulse, causing the local decrease in the density. A natural interpretation of the increase at short times is that additional energy deposited through interactions with the ablation plume leads to a slightly higher terminal velocity. Qualitatively, this type of behaviour is observed for a wide range of ablation power, valve voltage, valve-to-YAG timing and YAG-target alignment, though the detailed shape of the profile changes considerably.

Figure 3 shows the time-of-flight (TOF) profile ob-

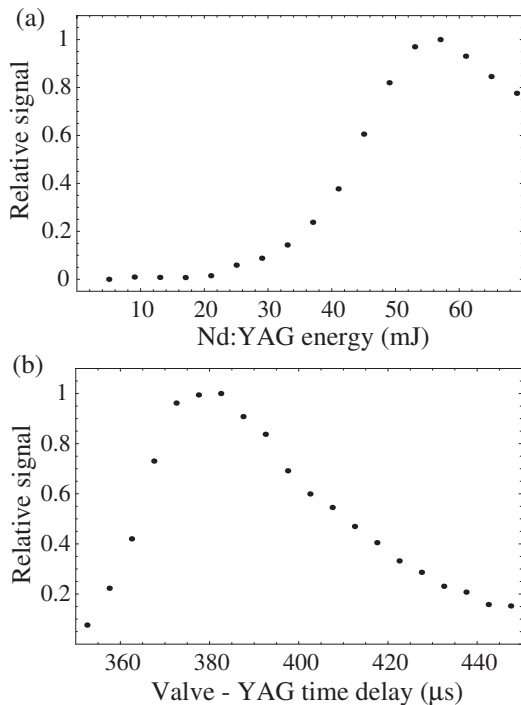


FIG. 4: Scaling of the ground-state LiH beam intensity with (a) Nd:YAG pulse energy and (b) time delay between valve trigger and Nd:YAG Q-switch trigger.

served at the LiH detector with the probe laser tuned to excite the ${}^7\text{Li}^1\text{H } A^1\Sigma^+(v' = 3) - X^1\Sigma^+(v'' = 0) R(0)$ transition at 805798 GHz. The signal is the average over 100 shots from the source, representing 10 seconds of integration time. The abscissa records the time since firing the ablation laser, while the ordinate gives the photon rate measured at the PMT. We fit a Gaussian (solid line) to the time-of-flight data, this being the expected profile when the translational temperature is low and the distribution formed at the source is narrow [22]. The molecules reach their terminal speed in a time much smaller than their total time-of-flight to the detector, and so the centre of the distribution immediately gives the mean speed. Since, as we show below, the pulse of molecules has a very narrow initial width ($\sim 5\mu\text{s}$), the width of the profile at the detector is an accurate measure of the translational temperature. The speed and translation temperature obtained from Fig. 3 are 628 m/s and 1.0 K respectively. We observe slow drifts in the speeds and temperatures obtained by this method which we attribute primarily to changes in target condition. Analyzing several datasets taken under nominally identical conditions many hours apart, we measure a mean speed of 625 ± 5 m/s, and a mean translational temperature of 0.9 ± 0.1 K. The velocity slip between the LiH and the carrier gas is a common feature of seeded molecular beams.

Figure 4(a) shows how the LiH signal varies with Nd:YAG pulse energy. The signal peaks at an ablation energy near 55 mJ per pulse, coinciding with the appear-

ance of the ‘hole’ in the gas pulse roughly as shown in Fig. 2. This observation suggests that the signal-limiting process involves a trade-off between the ablation yield and the preservation of the gas-pulse. At low energies the ablation yield, and hence the LiH signal, is small, while at high energies the ablation plume destroys the gas pulse, again leading to a small LiH signal. It follows that a pulsed valve delivering higher peak gas densities in correspondingly shorter pulses might yield higher LiH beam intensities.

There is a time delay between the valve trigger and the appearance of the gas pulse above the target due to the mechanical response of the solenoid valve. To optimize the LiH signal, the time delay between valve and YAG1 triggers needs to be chosen correctly. Figure 4(b), a plot of our signal as a function of this time delay, shows that the optimal delay is 385 μs . We note that this optimum is approximately 100 μs shorter than the delay used to centre the hole in the gas pulse, as in Fig. 2. This means that it is optimal to form the ablation plume when the leading edge of the gas pulse is above the target. Still shorter time delays result in higher translational temperatures as well as lower intensity.

By integrating under the TOF profile in Fig. 3 we measure the total number of photons detected per shot with the probe laser tuned to resonance. Figure 5(a) shows the data obtained upon scanning the laser frequency several times over a 1.2 GHz region around this resonance. The Gaussian fit to this data (solid line) gives a FWHM of 88 MHz, due to the Doppler width arising from the divergence of the detected beam. We observe very similar resonances when the laser is tuned through the $R(0)$ components of the corresponding $v' = 2$ and $v' = 4$ transitions at 795734.0 GHz and 816375.0 GHz respectively [16]. Figure 5(b) shows the same transition as in (a), but for the ${}^6\text{LiH}$ isotopic species. Taking into account the change of laser intensity between datasets (a) and (b), we determine the ratio of ${}^6\text{Li}$ to ${}^7\text{Li}$ in our source to be $7.7 \pm 0.5\%$, consistent with natural Li abundances. In order to determine the ground-state fraction in our beam, and hence the rotational temperature, we scanned over the ${}^7\text{LiH } R(1)$ resonance, as shown in Fig. 5(c). The sum of the squared matrix elements for this transition is twice that of the $R(0)$ line. Taking this, and the change of laser intensity into account, we find the population ratio between the ground and first rotationally excited states to be $N(J = 1)/N(J = 0) = 8.2 \pm 2.5\%$. Assuming thermal equilibrium amongst the rotational states, the corresponding rotational temperature is $T_{\text{rot}} = 5.9 \pm 0.5$ K, significantly hotter than the translational temperature. Furthermore, by analyzing the time-of-flight profiles, we observe that the $J = 1$ molecules have a speed that is 5.9 ± 1.3 m/s higher, and a translational temperature that is 0.25 ± 0.07 K higher than the $J = 0$ molecules in the same beam. This correlation indicates that the translational degree of freedom has not reached thermal equilibrium with the carrier gas and that the rotationally excited molecules are further from thermal equilibrium

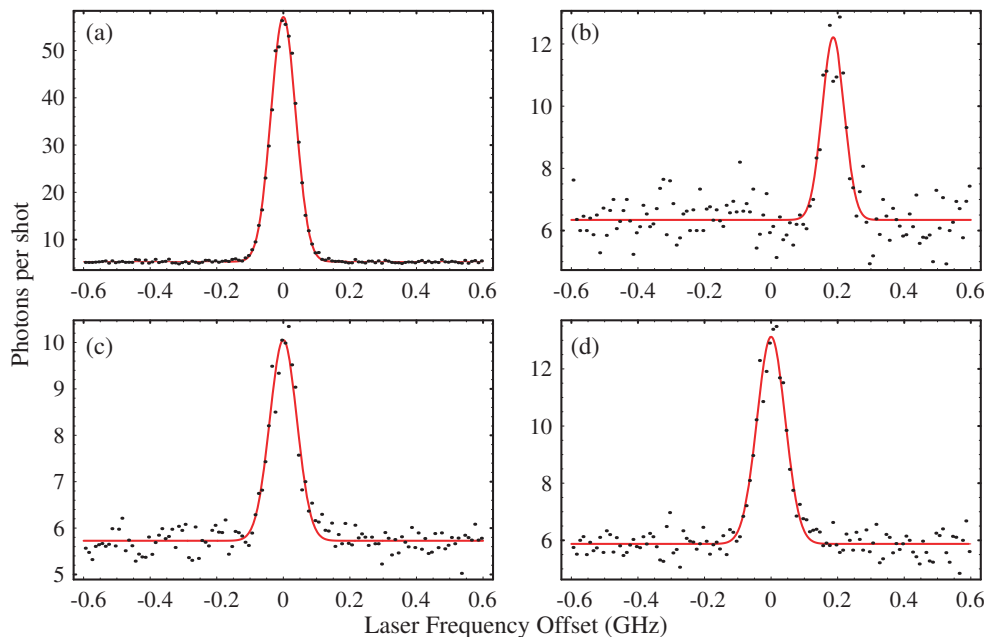


FIG. 5: Probe laser scans around the resonances $A^1\Sigma^+(v')-X^1\Sigma^+(v'')$ $R(J)$, along with Gaussian fits. (a) ${}^7\text{LiH}$, $v' = 3, v'' = 0, J = 0$, (b) ${}^6\text{LiH}$, $v' = 3, v'' = 0, J = 0$, (c) ${}^7\text{LiH}$, $v' = 3, v'' = 0, J = 1$ and (d) ${}^7\text{LiH}$, $v' = 6, v'' = 1, J = 0$. The central frequencies of these resonances, as recorded by a wavemeter with ± 600 MHz absolute accuracy, are (a) 805798.1 GHz, (b) 805966.4 GHz, (c) 805702.4 GHz and (d) 797837.6 GHz. These values are all in agreement with those tabulated in [16], or, where not tabulated, calculated from the set of mass-dependent Dunham coefficients given in the same reference.

than those in the ground state. A search for the $R(2)$ spectral line at 805336 GHz did not yield a signal, allowing us to set an upper bound on the population ratio $N(J=2)/N(J=0) < 4\%$. This is consistent with the rotational temperature determined above, but does not help to constrain its value further.

Turning now to the vibrations of the molecule, it is well known that this degree of freedom often decouples from the expansion at a much higher temperature than the others. To investigate this, we scanned the probe laser over the ${}^7\text{LiH } A^1\Sigma^+(v'=6)-X^1\Sigma^+(v''=1) R(0)$ transition, and obtained the data shown in Fig. 5(d). Knowing the laser intensities and the Franck-Condon factors [25], we deduce the population ratio between the first vibrationally excited state and the ground state to be $N(v''=1)/N(v''=0) = 1.5 \pm 0.2\%$. The corresponding vibrational temperature (assuming thermal equilibrium between the vibrations) is 468 ± 17 K. To investigate population in higher-lying vibrational levels, we scanned a 4 GHz region centred on the ${}^7\text{LiH } A^1\Sigma^+(v'=10)-X^1\Sigma^+(v''=2) R(0)$ transition at 804948 GHz, but did not observe a signal. The corresponding upper bound on the $v''=2$ population is $N(v''=2)/N(v''=0) < 1\%$, consistent with, but not further constraining, the above vibrational temperature.

Finally in this section, we mention that ablation at 355 nm, rather than at 1064 nm, does not change significantly the LiH signal obtained. We also note that we have not fully understood the LiH formation mechanism, particularly the role played by the H_2 in the carrier gas.

We find that decreasing the H_2 concentration does not result in a decreasing LiH signal. Indeed, the signal remains upon switching the carrier gas to pure argon, even after thoroughly flushing the gas-handling system. This puzzling observation suggests that it is hydrogen released from the target that is primarily responsible for LiH formation, rather than hydrogen present in the carrier gas.

B. Beam intensity

We now estimate the ground state LiH flux in our beam, using the signal measured on the $v' = 3 R(0)$ resonance. To ensure uniform laser power within the interaction volume, we expanded and collimated the probe beam and then selected the central portion using an aperture of height (along y) $H = 4$ mm and width (along z) $W = 3$ mm. The power passing through this aperture was $P = 2.3$ mW.

The number of photons detected per shot is given by

$$p = \frac{1}{L^2} \iint N(x, y) \epsilon(x, y) s(x, y) dx dy,$$

where $N(x, y)$, $\epsilon(x, y)$ and $s(x, y)$ are the number of ground state molecules per steradian, the detection efficiency and the number of photons scattered by each ground state molecule, all in the interval $dx dy$ around the point (x, y) in the plane of detection. L is the distance from source to detector. The values of N , ϵ and s are independent of y over the small interval defined by

the probe laser, H . At the laser intensity used, there is little power broadening, and only those molecules whose transverse Doppler shifts are within the natural linewidth contribute significantly to the signal. These molecules are confined to a small region about the beam axis within which N and ϵ are independent of x . With these simplifications, we have

$$p = N\epsilon(H/L^2)(L/v_z) \int s(v_x)dv_x,$$

where we have used the substitution $x = Lv_x/v_z$, v_x and v_z being the speeds in the x and z directions.

s is a strongly varying function of v_x due to the transverse Doppler shift. The upper state lifetime is much shorter than the time spent in the detector, and the probability of an excited molecule returning to the ground vibrational state is only 3%. It follows that the number of photons scattered by a molecule with transverse speed v_x is well approximated by $s(v_x) = 1 - \exp[-R(v_x)\tau]$, $R(v_x)$ being the excitation rate for this molecule, and τ the time taken to traverse the probe beam. When the laser is on resonance,

$$R\tau = \frac{D^2}{\epsilon_0 c \hbar^2} \frac{\gamma}{\Delta^2 + \gamma^2} \frac{P}{Hv_z}.$$

Here, $\Delta = 2\pi v_x/\lambda$ is the Doppler shift, $2\gamma = 32.4 \times 10^6 \text{ s}^{-1}$ is the natural linewidth of the transition [23], and $D^2 = |\langle A, v' = 3, J' = 1 | e z | X, v'' = 0, J'' = 0 \rangle|^2$ is the squared matrix element of the dipole operator between the initial and final states. The latter can be factored into a rotational part whose value is $1/3$ and an electronic-vibrational part whose value is $0.0486(ea_0)^2$ [25]. Evaluating the integral, we obtain $p = 6.6 \times 10^{-5} N\epsilon$.

The detection efficiency may be written as

$$\epsilon = (\Omega_l/4\pi) \sum_i q_i (1 + \mathcal{R}(\lambda_i)) T_l(\lambda_i)^2 T_w(\lambda_i) T_f(\lambda_i) \chi(\lambda_i).$$

Here, q_i is the fraction of fluorescent photons in the emission line whose wavelength is λ_i . \mathcal{R} , T_l , T_w , T_f and χ are respectively the wavelength-dependent mirror reflectivity, lens transmission, window transmission, filter transmission and PMT quantum efficiency. Ω_l is the solid angle subtended by the light-gathering lens (1.27 steradians). The result is $\epsilon = 0.96\%$ giving $p = 6.4 \times 10^{-7} N$. We measured $p = 29$ photons per shot, giving us $N = 4.5 \times 10^7$ molecules per steradian per shot. We estimate the relative uncertainty on this value to be $\pm 35\%$, taking into account the uncertainties in all the quantities involved in the calculation, including variations we observe from one target spot to another (which is the dominant contribution to the uncertainty).

The signal gradually decays as the ablated spot on the target ages, reaching half its initial value after about 20,000 shots.

C. Resonant excitation of the Li 2p state

As mentioned above, the reaction $\text{Li} + \text{H}_2 \rightarrow \text{LiH} + \text{H}$ is endothermic by 2.05 eV when the reactants are in the ground state. This value is reduced to 0.20 eV when the lithium is excited to the 2p state. It therefore seemed possible that excitation of the Li would result in an enhancement of the LiH yield. When investigating this reaction in a cell heated to approximately 800 K, Myers *et al.* [26] did indeed find a large enhancement of the reaction rate when the Li was resonantly excited on the D₁ and D₂ transitions at 670.8 nm; they measured the corresponding reaction cross-section to be $0.10 \pm 0.03 \text{ \AA}^2$. In our experiments, we scanned the frequency of a 10 mW diode laser over the D₁ and D₂ resonances and looked for an increase in the LiH yield. No such increase was observed, suggesting either that the reactants are sufficiently energetic for the reaction to proceed efficiently in the ground state, or that this reaction channel is not the main LiH production mechanism in the source.

D. Dual-pulse ablation

Recent literature on laser-induced breakdown spectroscopy (LIBS) of solid targets reports large signal enhancements when a dual-pulse ablation scheme is used (e.g. [27] and references therein). Typically, the two pulses are temporally separated by a few μs . Enhancements are reported for co-linear geometries where both laser beams hit the target, and in orthogonal geometries where one beam travels over the surface of the target, which the other hits. The underlying mechanisms for these enhancements are the focus of current research in this area. Since our own experimental setup shares some features with the LIBS technique, we searched for a similar signal enhancement using the (near) co-linear dual-pulse arrangement shown in Fig. 1.

We scanned the time-delay between the firing of YAG1 and YAG2, modulating YAG2 on and off so as to obtain the ratio of dual-pulse to single-pulse LiH beam intensity at each time delay. The single-pulse signal was first optimized with respect to YAG1 energy, YAG2 energy, position on the target and time-delay between the valve and YAG1 triggers. Figure 6 shows typical results. The data were taken with energies and spot sizes of 42 mJ, 4 mm (YAG1) and 19.5 mJ, 2 mm (YAG2). Figure 6(a) shows the signal ratio as a function of the time delay scanned with $2 \mu\text{s}$ resolution. Over most of the interval from -10 to +40 μs , there is a clear increase in the signal with the addition of YAG2. We believe this is due to the formation of a second LiH cloud in a different part of the gas pulse: each plume interacts with only a narrow ($\sim 5 \mu\text{s}$) slice of the gas. This idea is supported by the $5 \mu\text{s}$ wide region near zero time delay where there is no increase in the signal. Here, the second plume has little effect because the gas is already optimally depleted by the first, as discussed in the context of Fig. 4(a). The

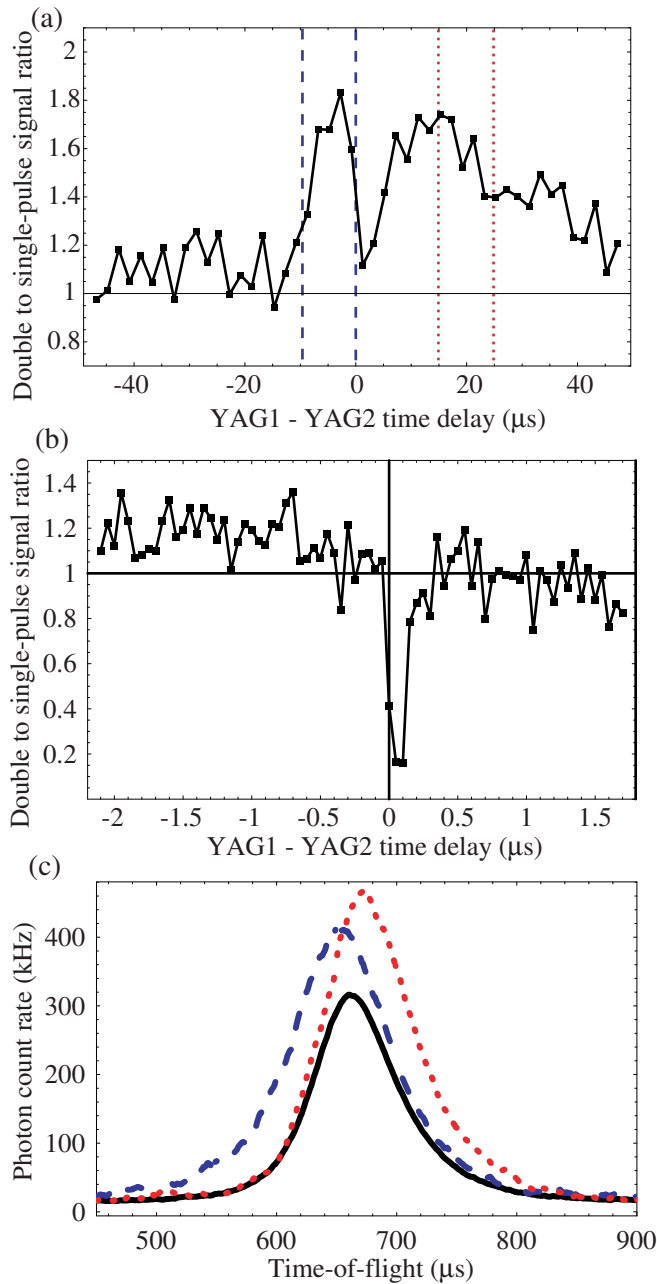


FIG. 6: Dual-pulse ablation results. (a) Double-pulse to single-pulse signal ratio as a function of the time delay between the two ablation pulses scanned with $2\mu\text{s}$ resolution. (b) As (a), but with 50 ns resolution in the interval around zero time-delay. (c) Time-of-flight profiles for single-pulse ablation (solid line), dual-pulse ablation with time-delays between $-10\mu\text{s}$ and $0\mu\text{s}$ (dashed line) and with time-delays between $15\mu\text{s}$ and $25\mu\text{s}$ (dotted line).

asymmetry between negative and positive time-delays in Fig. 6(a) arises because the pulse from YAG1 interacted with the early part of the gas pulse, rather than the central part (as discussed above, this choice optimizes the single-pulse intensity).

We re-scanned the region around zero time delay with

50 ns resolution. This revealed the much narrower dip shown in Figure 6(b), when the first and second YAG pulses coincide within 250 ns. The signal decreases to about 20% of the single-pulse value because the effective ablation intensity is approximately twice the optimum value when the two pulses hit the target almost simultaneously. We have observed much broader signal-drops at higher values of YAG2 energy.

For each data point in Figs. 6(a,b) there is a corresponding time-of flight profile. In 6(c), the solid line shows the TOF profile measured for single-pulse ablation. The dashed line shows the dual-pulse TOF profile averaged over the data points between $-10\mu\text{s}$ and $0\mu\text{s}$ (the region between the dashed lines in (a)), while the dotted line is the corresponding average for the interval $15\mu\text{s}$ to $25\mu\text{s}$ (indicated by dotted lines in (a)). We see that when YAG2 fires before YAG1 the profile is broadened on the early-arrival side, and when it fires later it is broadened on the late-arrival side. The molecules leave the source as two separate pulses which, due to their finite temperature, merge into a single broadened pulse as they travel down the beamline. When YAG2 is delayed by more than $50\mu\text{s}$, we observe two distinct peaks in the TOF.

E. Long-pulse ablation

The logical extension of dual-pulse ablation is multi-pulse, or long-pulse ablation, with a pulse length chosen to match the duration of the gas pulse. In this way, the entire gas pulse would contribute to the molecular signal. One convenient way to achieve this is to operate the Nd:YAG laser without a Q-switch. In this case, the laser undergoes relaxation oscillations emitting a pulse train that lasts for approximately $150\mu\text{s}$ and consists of approximately 100 pulses, each of $\sim 1\mu\text{s}$ duration. The total energy output is roughly the same as in Q-switched mode.

In order to observe a LiH signal in this mode, we found it necessary to compensate for the much lower ablation power by focussing the laser onto the target using a lens placed one focal length (500 mm) away from the target. We then observed a ground-state LiH signal whose intensity increased with increasing ablation energy up to the maximum energy available. The maximum size of the signal obtained was approximately 15 times larger than in Q-switched mode. Because of the much broader temporal distribution of molecules at the source, we are not at present able to comment on the translational temperature. The greatly increased signal is accompanied by very large fluctuations on the timescale of tens of seconds. We attribute these fluctuations to the drastic changes in surface conditions that occur as the tightly focussed ablation laser forms deep holes and broad craters in the target. Initial experiments indicate that these large fluctuations can be minimized by continuously translating the target. We are currently modifying our source so as to take full

advantage of the much larger signals obtainable in this long-pulse mode.

F. Conclusions

We have produced a beam of LiH with a translational temperature below 1 K. We observe a number of non-equilibrium effects in our beam: velocity slip, a rotational temperature higher than the translational temperature, an even higher vibrational temperature, and a rotational-state dependence on the speed and translational temperature. Despite these effects, the majority of the molecules are cooled to the ground state. In a first step towards increased beam intensity, we find that long-pulse ablation produces a far higher flux than single-pulse ablation, due to a more uniform loading of the carrier gas pulse. We are exploring several promising avenues to increase the

intensity further - various targets and hydrogen donor gases, ablation inside an extended nozzle, and electrical discharge to dissociate the molecular hydrogen. We plan to use our cold LiH beam in deceleration and trapping experiments, with a view to reaching sub-mK temperatures using a second-stage cooling scheme such as sympathetic cooling [28] or cavity-assisted cooling [29].

Acknowledgments

We are indebted to Jon Dyne for his expert technical assistance, and to Gerard Meijer, Irena Labazan and Tim Steimle for very valuable discussions. We acknowledge UK support from the Royal Society, EPSRC and PPARC, and the Cold Molecules Network of the European Commission.

-
- [1] J. Doyle, B. Friedrich, R.V. Krems and F. Masnou-Seeuws, *Eur. Phys. J. D* **31**, 149 (2004)
 - [2] H.L. Bethlem and G. Meijer, *Int. Rev. Phys. Chem.* **22**, 73 (2003)
 - [3] H.L. Bethlem, G. Berden and G. Meijer, *Phys. Rev. Lett.* **83**, 1558 (1999)
 - [4] H.L. Bethlem, G. Berden, F.M.H. Crompvoets, R.T. Jongma A.J.A. van Roij and G. Meijer, *Nature* **406**, 491 (2000); H.L. Bethlem, F.M.H. Crompvoets, R.T. Jongma, S.Y.T. van de Meerakker and G. Meijer, *Phys. Rev. A* **65**, 053416 (2002)
 - [5] F.M.H. Crompvoets, H.L. Bethlem, R.T. Jongma and G. Meijer, *Nature* **411**, 174 (2001)
 - [6] J.R. Bochinski, E.R. Hudson, H.J. Lewandowski, G. Meijer and J. Ye, *Phys. Rev. Lett.* **91**, 243001 (2003)
 - [7] S.Y.T. van de Meerakker, P.H.M. Smeets, N. Vanhaecke, R.T. Jongma and G. Meijer, *Phys. Rev. Lett.* **94**, 023004 (2005)
 - [8] S.Y.T. van de Meerakker, I. Labazan, S. Hoekstra, J. Küpper and G. Meijer, *J. Phys. B* **39**, S1077 (2006)
 - [9] E. R. Hudson, C. Ticknor, B. C. Sawyer, C. A. Taatjes, H. J. Lewandowski, J. R. Bochinski, J. L. Bohn and J. Ye, *Phys. Rev. A* **73**, 063404 (2006).
 - [10] M.R. Tarbutt, H.L. Bethlem, J.J. Hudson, V.L. Ryabov, V.A. Ryzhov, B.E. Sauer, G. Meijer, and E.A. Hinds, *Phys. Rev. Lett.* **92**, 173002 (2004)
 - [11] C. R. Vidal and W. C. Stwalley, *J. Chem. Phys.* **77**, 883 (1982)
 - [12] M. Bellini, P. De Natale, M. Inguscio, T. D. Varberg and J. M. Brown, *Phys. Rev. A* **52**, 1954 (1995)
 - [13] E. Bodo, F. A. Gianturco and R. Martinazzo, *Phys. Rep.* **384**, 85 (2003)
 - [14] D.Puy and M. Signore, *New Astronomy* **3**, 27 (1998)
 - [15] W.C. Stwalley and W. T. Zemke, *J. Phys. Chem. Ref. Data* **22**, 87 (1993)
 - [16] N. Bouloufa, P. Cacciani, R. Vetter and A. Yiannopoulou, *J. Mol. Spec.* **202**, 37 (2000)
 - [17] M. Dulick, K. -Q. Zhang, B. Guo and P. F. Bernath, *J. Mol. Spec.* **188**, 14 (1998)
 - [18] W. C. Lin, J. J. Chen and W. T. Luh, *J. Phys. Chem. A* **101**, 6709 (1997)
 - [19] J. J. Chen, W. T. Luh and G. H. Jeung, *J. Chem. Phys.* **110**, 4402 (1999)
 - [20] P. J. Dagdigian, *J. Chem. Phys.* **64**, 2609 (1976)
 - [21] "Bond Dissociation Energies", in *CRC Handbook of Chemistry and Physics*, 87th Edition, D.R. Lide, ed., Taylor and Francis, Boca Raton, FL (2007)
 - [22] M.R. Tarbutt, J.J. Hudson, B.E. Sauer, E.A. Hinds, V.A. Ryzhov, V.L. Ryabov and V.F. Ezhov, *J. Phys. B* **35**, 5013 (2002)
 - [23] W.T. Zemke, J.B. Crooks and W.C. Stwalley, *J. Chem. Phys.* **68**, 4628 (1978)
 - [24] I. Labazan, N. Krstulović and S. Milošević, *Chem. Phys. Lett.* **428**, 13 (2006)
 - [25] W.T. Zemke and W.C. Stwalley, *J. Chem. Phys.* **68**, 4619 (1978)
 - [26] E.G. Myers, D.E. Murnick and W.R. Softky, *Appl. Phys. B* **43**, 247 (1987)
 - [27] V. Hohreiter and D.W. Hahn, *Spectrochim. Acta B* **60**, 968 (2005)
 - [28] M. Lara, J. L. Bohn, D. Potter, P. Soldán and J. M. Hutson, *Phys. Rev. Lett.* **97**, 183201 (2006)
 - [29] P. Domokos and H. Ritsch, *Phys. Rev. Lett.* **89**, 253003 (2002)